The Plant Cell, Vol. 28: 87–101, January 2016, www.plantcell.org

Complementary Activities of TELOMERE REPEAT BINDING Proteins and Polycomb Group Complexes in Transcriptional Regulation of Target Genes[OPEN]

Yue Zhou, Benjamin Hartwig, Geo Velikkakam James,[1] Korbinian Schneeberger, and Franziska Turck[2]

Department Plant Developmental Biology, Max Planck Institute for Plant Breeding Research, 50829 Köln, Germany

ORCID IDs: 0000-0002-2507-7990 (Y.Z.); 0000-0002-5512-0443 (K.S.); 0000-0002-4982-5949 (F.T.)

In multicellular organisms, Polycomb Repressive Complex 1 (PRC1) and PRC2 repress target genes through histone modification and chromatin compaction. *Arabidopsis thaliana* mutants strongly compromised in the pathway cannot develop differentiated organs. LIKE HETEROCHROMATIN PROTEIN1 (LHP1) is so far the only known plant PRC1 component that directly binds to H3K27me3, the histone modification set by PRC2, and also associates genome-wide with trimethylation of lysine 27 of histone H3 (H3K27me3). Surprisingly, *lhp1* mutants show relatively mild phenotypic alterations. To explain this paradox, we screened for genetic enhancers of *lhp1* mutants to identify novel components repressing target genes together with, or in parallel to, LHP1. Two enhancing mutations were mapped to *TELOMERE REPEAT BINDING PROTEIN1* (*TRB1*) and its paralog *TRB3*. We show that TRB1 binds to thousands of genomic sites containing *telobox* or related *cis*-elements with a significant increase of sites and strength of binding in the *lhp1* background. Furthermore, in combination with *lhp1*, but not alone, *trb1* mutants show increased transcription of LHP1 targets, such as floral meristem identity genes, which are more likely to be bound by TRB1 in the *lhp1* background. By contrast, expression of a subset of LHP1-independent TRB1 target genes, many involved in primary metabolism, is decreased in the absence of *TRB1* alone. Thus, TRB1 is a bivalent transcriptional modulator that maintains downregulation of Polycomb Group (PcG) target genes in *lhp1* mutants, while it sustains high expression of targets that are regulated independently of PcG.

INTRODUCTION

Polycomb Group (PcG) proteins epigenetically regulate cell fate and identity in higher eukaryotes by chromatin-mediated gene repression. PcG proteins form functionally distinct complexes that act in concert to modify chromatin by trimethylation of lysine 27 of histone H3 (H3K27me3) and monoubiquitination of a lysine residue within the histone fold domain of H2A (H2Aub). Occurrence of these two hallmark modifications leads to local chromatin compaction and gene repression by mechanisms that are not yet entirely understood (Schuettengruber and Cavalli, 2009; Margueron and Reinberg, 2011; Xiao and Wagner, 2015).

In *Arabidopsis thaliana*, two Polycomb repressive complexes (PRCs) have been identified, both of which exist in multiple variants due to gene family expansion and functional diversification (Derkacheva and Hennig, 2014). PRC2 sets the H3K27me3 mark, which covers around 4400 to 7000 genes, depending on tissue type and target threshold definition used in several independent genome-wide studies (Zhang et al., 2007b; Weinhofer et al., 2010; Lafos et al., 2011; Dong et al., 2012). PRC1 fulfils three molecular functions that may not depend on a single holocomplex, but could be implemented by PRC1-like subcomplexes (Mozgova and Hennig, 2015). PRC1 component LIKE HETEROCHROMATIN PROTEIN1 (LHP1) can recognize H3K27me3 through its chromodomain (Turck et al., 2007; Zhang et al., 2007a; Exner et al., 2009), while H2A monoubiquitination is dependent on the presence of RING-RAWUL twin domain proteins of the Arabidopsis B Lymphoma Mo-MLV Insertion Region 1 and RING FINGER PROTEIN1 subfamily (Bratzel et al., 2010; Yang et al., 2013; Calonje, 2014). Finally, EMBRYONIC FLOWER1 (EMF1) is a PRC1 component likely involved in chromatin compaction (Calonje et al., 2008; Beh et al., 2012). Genome-wide binding studies have been performed for both LHP1 (Turck et al., 2007; Zhang et al., 2007a; Engelhorn et al., 2012) and EMF1 (Kim et al., 2012) and suggested an overlapping binding pattern strictly correlated to the occurrence of H3K27me3.

LHP1 loss-of-function mutants show pleiotropic phenotypes, including early flowering, upward leaf curling, reduced leaf size, and dwarfism (Larsson et al., 1998; Gaudin et al., 2001; Kotake et al., 2003). The collective upregulation of MADS domain transcription factors encoded by the *ABCDE* floral meristem identity genes, such as *SEPALLATA3* (*SEP3*), *APETALA1* (*AP1*), *AP3*, *AGAMOUS* (*AG*) and *SHATTERPROOF1*, explains part of the *lhp1* mutant phenotype, although it is rather difficult to disentangle the effects directly caused by the lack of LHP1-mediated repression from those due to the mutual upregulation within the regulatory network (Nakahigashi et al., 2005; Derkacheva et al., 2013). In addition, both the floral repressor *FLOWERING LOCUS C* (*FLC*) and *FLOWERING LOCUS T* (*FT*), encoding the photoperiod-dependent florigen, are upregulated in *lhp1* mutants (Takada and Goto, 2003; Mylne et al., 2006; Sung et al., 2006). FLC is a direct

[1] Current address: Rijk Zwaan R&D Fijnaart, 4793 RS Fijnaart, The Netherlands.
[2] Address correspondence to turck@mpipz.mpg.de.
The author responsible for distribution of materials integral to the findings presented in this article in accordance with the policy described in the Instructions for Authors (www.plantcell.org) is: Franziska Turck (turck@mpipz.mpg.de).
[OPEN]Articles can be viewed online without a subscription.
www.plantcell.org/cgi/doi/10.1105/tpc.15.00787

repressor of *FT*, but in the *lhp1* mutant, *FT* is upregulated in phloem companion cells despite increased *FLC* levels, explaining most of the early flowering phenotype (Kotake et al., 2003; Searle et al., 2006; Farrona et al., 2011b).

LHP1 directly interacts with RING-RAWUL proteins and EMF1, indicating that LHP1 can be present in several PRC1-like complexes (Xu and Shen, 2008; Bratzel et al., 2010). In addition, LHP1 was detected in pull-down experiments performed using epitope-tagged MSI1 as bait due to a direct interaction with MSI1 (Derkacheva et al., 2013). It was suggested that recruitment of PRC2 by H3K27me3-bound LHP1 is important to maintain H3K27me3 levels in root cultures undergoing rapid cell division (Derkacheva et al., 2013).

Recent reports suggest that PRC1 can at least sometimes act upstream of PRC2 since H2Aub preceded H3K27me3 during postgerminative repression of seed maturation genes (Bratzel et al., 2010; Yang et al., 2013; Calonje, 2014). In theory, LHP1 would be able to mediate the connection between PRC1-like complexes and PRC2 in the absence of H3K27me3 in this scenario. Moreover, in vitro, Arabidopsis *GAGA*-motif binding factors, such as BASIC PENTACYSTEINE6 (BPC6), can recruit PRC1 to *GAGA* motifs by their direct interaction with LHP1, which may subsequently recruit PRC2 (Hecker et al., 2015). Other transcription factors, such as SHORT VEGETATIVE PHASE and SHORT ROOT, were shown to interact with LHP1 and, likewise, may be involved in triggering PcG-mediated repression at their target genes (Cui and Benfey, 2009; Liu et al., 2009).

Despite the central position of LHP1 in PRC1 and its high connectivity to PRC2, the role of LHP1 within the PcG pathway remains a conundrum. LHP1, in contrast to most PRC1 and 2 components, is encoded by a single copy gene in Arabidopsis, for which true null alleles are available. Nevertheless, the *lhp1* phenotype is mild compared with other more severe PcG mutants (Mozgova and Hennig, 2015). For example, a combination of mutations in *CURLY LEAF* and *SWINGER*, which together provide all sporophytic H3K27me3-directed activity (Farrona et al., 2011b; Lafos et al., 2011), leads to much more severe developmental defects. After germination, *clf swn* mutant plants develop a transdifferentiating cell clump that initiates organ development, including the formation of somatic embryos, without ever progressing to organ maturity (PcG callus) (Chanvivattana et al., 2004). A PcG callus is also observed in Arabidopsis mutants severely affected in H2Aub activity, such as triple *bmi1a bmi1b bmi1c* or double *ring1a ring1b* mutants (Chen et al., 2010; Yang et al., 2013). These observations indicate that there may be other proteins or pathways acting either redundantly or in parallel with LHP1.

Here, we report on results of a forward genetic screen for genetic enhancers of the *lhp1* phenotype that we performed to uncover such novel components. We mapped mutations in genes coding for Myb-family transcription factor TELOMERE REPEAT BINDING PROTEIN1 (TRB1) and the related TRB3 as causal enhancers of the *lhp1* phenotype. We show by genome-wide expression (RNA-seq) and chromatin immunoprecipitation sequencing (ChIP-seq) analysis that TRB1, by binding to *teloboxes* and *telobox*-related *cis*-elements, plays a role in transcription regulation that is independent of its previously identified role in telomere maintenance (Schrumpfova et al., 2014). Interestingly, TRB1 assists LHP1 in the repression of common target genes, while for a set of genes predominantly involved in primary metabolism, TRB1 binding seems to be required to sustain high expression levels. Finally, we discuss several functional models that would fit our observations.

RESULTS

Identification of Genetic Enhancers of *lhp1*

We induced mutations in the *lhp1-3* mutant background (from now *lhp1*) by ethyl methanesulfonate (EMS) and screened for genetic enhancers. Two nonallelic *lhp1* enhancers showing earlier flowering and stronger leaf size reduction (Figures 1A to 1C) were mapped by fast isogenic mapping (Hartwig et al., 2012) to the *TRB1* and *TRB3* loci (Supplemental Table 1). Mapping of causative mutations was validated by full complementation of the enhancer mutants by the corresponding genomic fragments and a reproduction of the enhanced phenotype after introducing independent T-DNA insertion alleles *trb1-2* and *trb3-2* in the *lhp1* background (Supplemental Figures 1A to 1E). Note that both T-DNA alleles express a partial transcript encoding the MYB domain of TRB1 and 3; therefore, partial activity of the encoded proteins may be retained (Supplemental Figure 1D).

TRB1 and TRB3 feature an N-terminal single repeat Myb domain and a C-terminal domain related to linker histones H1 and H5 (Supplemental Figure 1C). This domain structure is shared by five Arabidopsis proteins belonging to two distinct clades that formed at the origin of seed plants (Supplemental Figure 2A and Supplemental Data Set 1). The TRB clade of Arabidopsis Myb-domain proteins contains three members, which form hetero- and homomultimers (Kuchar and Fajkus, 2004). Histochemical data showed that *TRB1* and *TRB3* are expressed throughout the plant (Supplemental Figure 3), suggesting that they have not subfunctionalized by evolving distinct tissue-specific expression patterns. In the wild-type background, single and combined loss of *TRB1* and *TRB3* did not result in obvious phenotypic alterations, supporting the notion of functional redundancy between the factors (Figures 1A to 1C). By contrast, triple *trb1-1 trb3-1 lhp1* mutants showed stronger *lhp1* enhancement than both double mutants, indicating that *TRB1* and *TRB3* are only partially redundant in the sensitized *lhp1* background (Figures 1A to 1C).

The *trb1-1* and *trb3-1* alleles changed conserved codons within the Myb domain to encode phenylalanine instead of leucine and glutamic acid instead of glycine, respectively (Supplemental Figure 2B). TRBs were previously shown to bind plant telomere repeat sequences (Schrumpfova et al., 2004; Hofr et al., 2009). Compared with the wild-type version, proteins encoded by *trb1-1* fused to *GFP* showed a loss of fluorescence foci in the nucleoplasm (Figure 1D, green channel, two left-most panels). Based on previous colocalization studies in the same experimental system, these foci overlap with telomere repeat regions detected by DNA-fluorescence in situ hybridization (Schrumpfova et al., 2014). By contrast, an enrichment at the nucleolus was still shared between the mutant and wild-type TRB1:GFP fusions (Figure 1D, two left-most panels). Thus, localization within the nucleolus may be independent of specific DNA binding mediated by the Myb domain. TRB3-1:GFP levels were strongly reduced compared with wild-type TRB3:GFP, indicating rapid turnover of the mutated protein (Figure 1D, red channel, first and second rows). In contrast to TRB1 and TRB3, LHP1 was neither particularly enriched nor depleted at

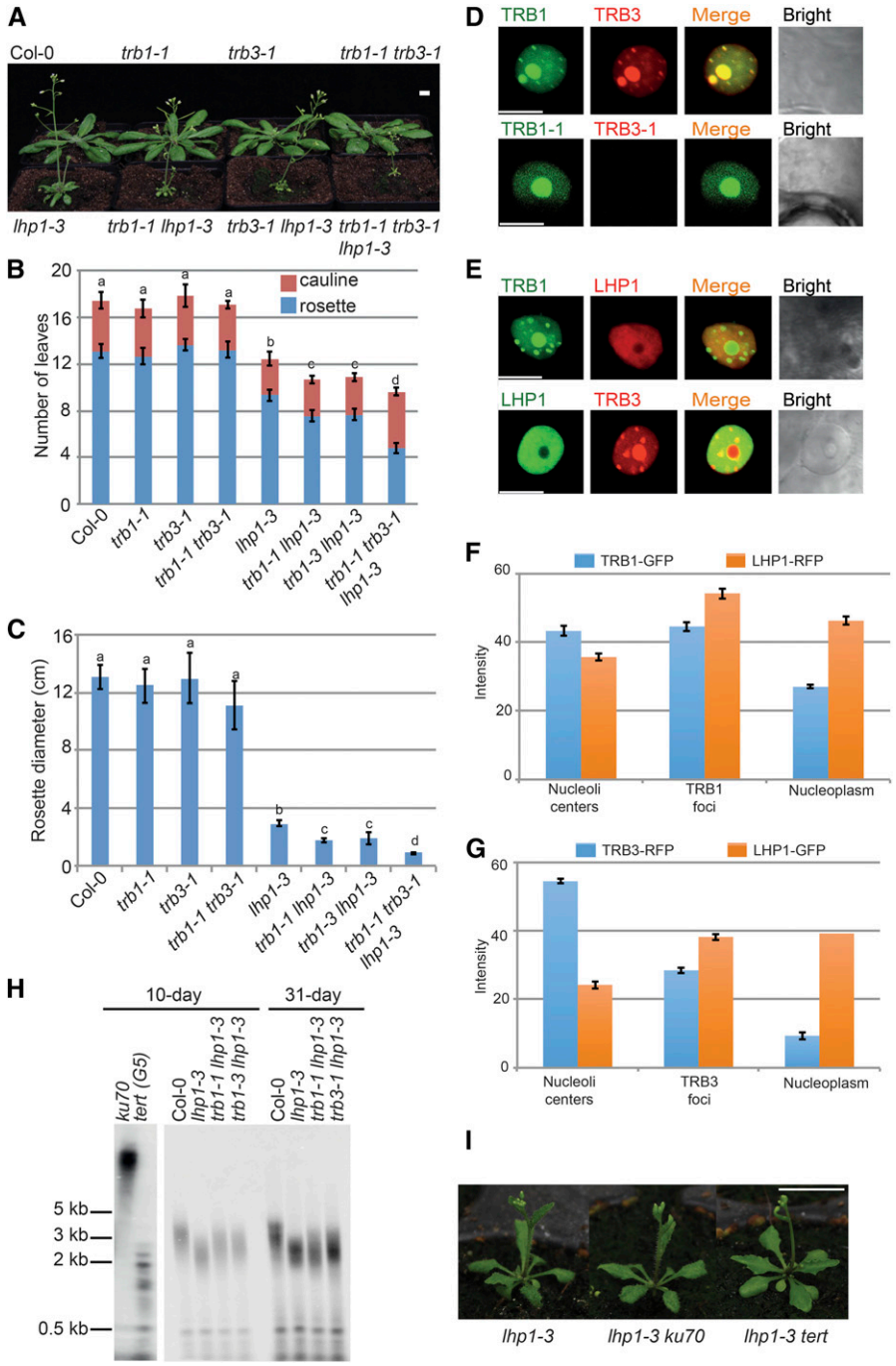

Figure 1. *trb1* and *trb3* Alleles Enhance the *lhp1* Mutant Phenotype Independently of Their Role in Telomere Maintenance.

(A) Phenotype of Col-0, *trb1-1*, *trb3-1*, *trb1-1 trb3-1*, *lhp1-3*, *trb1-1 lhp1-3*, *trb3-1 lhp1-3*, and *trb1-1 trb3-1 lhp1-3* plants 28 d postgermination. Plants were grown at 22°C in long days. Bar = 1 cm.

(B) Flowering time of genotypes grown as in **(A)** scored as number of leaves. Error bars indicate mean ± SE ($n = 9$). Statistical significance was determined by one-way ANOVA with multiple comparison correction by Tukey HSD. Different letters indicate significance groups ($P < 0.001$).

(C) Rosette size of plants as in **(B)**; statistical significance tested as above.

(D) Localization of fluorescent TRB1 and TRB3 wild-type and mutant fusion proteins transiently produced in tobacco leaves. Bar = 10 μm.

(E) Colocalization of fluorescent TRB1, TRB3, and LHP1 fusion proteins transiently produced in tobacco leaves Bar = 10 μm.

(F) Average intensity of TRB1-GFP and LHP1-RFP across regions of interest. Error bars represent Student's *t* test confidence intervals ($n = 9$).

(G) Average intensity of TRB3-RFP and LHP1-GFP as in **(F)**.

TRB1 and TRB3 foci (Figures 1E to 1G; Supplemental Figure 4). As previously reported (Libault et al., 2005), LHP1 was relatively depleted at the centers of nucleoli (Figures 1E to 1G; Supplemental Figure 4). Thus, colocalization of both TRBs with LHP1 appeared throughout the nucleoplasm, including TRB1 and TRB3 foci, while it is less probable at the nucleolus due to the relative depletion of LHP1.

Enhancement of *lhp1* by Mutations in *trb1* and *trb3* Is Independent of Telomere Function

Successive generations of Arabidopsis plants carrying *telomerase* (*tert*) loss-of-function alleles show progressive telomere shortening, which is perceptible from the first generation on. Until generation 5, telomere shortening in *tert* mutants has no phenotypic consequences, but from that point on developmental aberrations accumulate, resulting in phenotypes that resemble strong PcG loss-of-function mutants (Riha et al., 2001). A T-DNA insertion allele in TRB1 resulted in a mild reduction (10 to 20%) in telomere length after five generations, but had no phenotypic effect (Schrumpfova et al., 2014).

To investigate whether enhancement of the *lhp1* phenotype by *trb1* and *trb3* could be explained by an accelerated pace of telomere degeneration, we measured telomere length in the relevant mutants. Irrespective of their age, seedlings or mature *lhp1*, *trb1-1 lhp1*, and *trb3-1 lhp1* plants of the first homozygous generation had telomeres in the wild-type length range of 2 to 5 kb. This range is different from the respectively long and short telomeres of *ku70* and *tert* mutants of the fifth generation, but not from wild-type (Col-0) telomeres that were used as reference (Figure 1H) (Riha et al., 2001; Riha and Shippen, 2003). Thus, phenotypic enhancement in *trb1-1 lhp1* and *trb3-1 lhp1*, which is visible from the first generation, precedes visible telomere shortening, excluding the possibility that a role of TRBs in telomere homeostasis enhances the *lhp1* phenotype. In general, the PcG pathway does not seem to play a role in telomere homeostasis, since telomere length was not affected in plants with mutations in several other PRC1 and PRC2 components, although these mutants had been homozygous for several generations (Supplemental Figure 5). In addition, altered telomere length did not influence the *lhp1* phenotype, since *ku70 lhp1* and *tert lhp1* double mutants of the first homozygous generation had a phenotype similar to *lhp1* (Figure 1I).

Misexpression of Floral Meristem Identity Genes Is Enhanced in *trb1-1 lhp1* Double Mutants Compared with *lhp1* Single Mutants

We profiled the transcriptome of *trb1-1* and *lhp1* single and double mutants by RNA-seq to uncover TRB1-related functions that would explain the observed *lhp1* enhancement (see Supplemental Data Set 2 for all and Supplemental Data Set 3 for an overview of differentially expressed genes). Although phenotypically indistinguishable from the wild type, the number of misregulated genes in *trb1-1* was comparable to those in *lhp1* single and *trb1-1 lhp1* double mutants (Figure 2A). To test how misregulation correlated to PcG-mediated repression, we overlapped the gene sets with a list of H3K27me3 target genes determined by ChIP-seq analysis. PcG target genes were not overrepresented in scenarios that included the *lhp1* mutant (Fisher's test $P < 2.36e-01$ and $P < 9.04e-02$ for *lhp1* and *trb1 lhp1*, respectively). Although this may seem unexpected, it fits well with the observation that *lhp1* shows a relatively mild phenotype not in accordance with a general misregulation of PcG target genes. PcG target genes were underrepresented in the set misregulated in *trb1-1* (Fisher's test $P < 9.21e-08$; Figure 2B).

Misregulation of 83 genes was common to both *trb1-1* and *lhp1* single mutants, and of these misregulated genes, 53 were also misregulated in *trb1-1 lhp1* double mutants, which shared 79 genes with *trb1-1* alone (Figure 2A). Although many of these commonly misregulated genes shared the direction of change observed in the wild type, the sets did not contain obvious candidate genes that would directly link to the phenotype, making it less likely that genetic enhancement was due to additive effects. Nonadditive phenotypic enhancement in the double mutant could either be attributed to genes that newly appeared in the misregulated set of *trb1-1 lhp1* double mutants or to those already affected in *lhp1*, but increasingly so in the double mutants. Many of the 144 genes misregulated in *trb1-1 lhp1*, but not in *lhp1*, were connected to photosynthesis rather than developmental functions, which made the latter the more plausible scenario (Supplemental Data Set 3). Indeed, *AG*, *AP3*, and, to a lesser degree, *SEP3* were further upregulated in *trb1-1 lhp1* compared with *lhp1*, suggesting that they may play a role in phenotypic enhancement (Supplemental Data Set 3). We evaluated the expression of *AG*, *AP3*, *SEP3*, and *FT* directly by qRT-PCR, which corroborated that floral meristem identity genes showed increased expression in *trb1-1 lhp1* compared with *lhp1* (Supplemental Figure 6).

TRB1 Affects Photosynthesis-Related Genes Alone and Developmental Regulatory Genes Together with *LHP1*

Since the quality of the gene set misregulated in *trb1-1* alone seemed distinct from the one likely linked to phenotypic enhancement of *lhp1*, we performed further transcriptional pattern and Gene Ontology (GO) term enrichment analysis to uncover functional connections among groups of misregulated genes (Figure 2C; Supplemental Data Sets 3 and 4). Preliminary analysis showed that median normalization and the number of $k = 8$ lead to robust k-clustering results. Three of the clusters (1, 6, and 8) were predominantly affected by the *lhp1* mutation with cluster 1 showing anticorrelation to clusters 6 and 8. Misexpression in cluster 6 was most obviously enhanced in the *trb1-1 lhp1* double mutant background. Two clusters (2 and 5) were predominantly affected in the *trb1-1* background, showing misregulation in the

Figure 1. (continued).

(H) Telomere length analysis. DNA was prepared from Col-0, *lhp1-3*, *trb1-1 lhp1-3*, and *trb3-1 lhp1-3* pools of (100 to 200) 10-d-old seedlings and 31-d-old individual plants. Material from 10-d-old *ku70* and *tert* (G5) seedlings was included as reference.
(I) Phenotype of *lhp1-3*, *ku70 lhp1-3*, and *tert lhp1-3*. Bar = 1 cm.

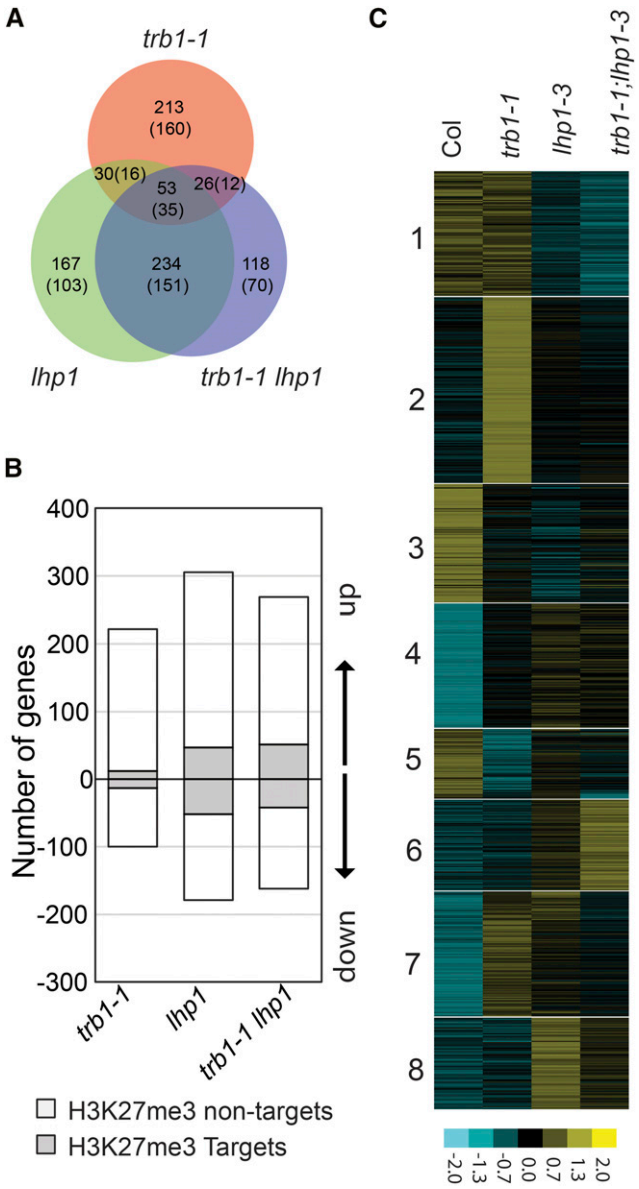

Figure 2. Effect of Mutation of *TRB1* on Gene Expression in Seedlings.

(A) Venn diagram of genes differentially regulated in *trb1-1*, *lhp1-3*, and *trb1-1 lhp1-3* seedlings compared with wild-type Col based on RNA-seq data (biological replicates $n = 3$, Baggerley's test with FDR correction on RPKM values per gene, threshold FDR < 0.05, fold change > 2). Comparison only for upregulated genes indicated in parentheses.

(B) Number of genes up- or downregulated in each genotype. Proportion of H3K27me3 target genes indicated in gray.

(C) Transcriptional clustering of misregulated genes. K-median (k = 8) clustering after median centering each gene across all samples (arbitrary units). A representative clustering result is shown.

opposite direction. In clusters 3, 4, and 7, expression in the wild type was most distinct from all mutant backgrounds, indicating that gene expression was affected by *trb1-1* and *lhp1* in similar direction.

The clusters strongly diverged in their average expression levels as estimated by average read count (Figure 3A). PcG target genes were overrepresented in clusters with low and virtually absent in clusters with high read count (Figure 3B; Supplemental Data Set 3). In conclusion, genes affected by mutation of *TRB1* belonged to two distinct groups. Highly expressed genes were affected by *trb1-1* as a single mutation (clusters 2 and 5), while increased upregulation of a lowly expressed subset containing many PcG target genes was observed in combination with *lhp1* (cluster 6).

We used hierarchical clustering to further analyze whether the k groups shared enriched GO terms (Figure 3C; Supplemental Data Set). Functional connections were most significant for clusters 2, 5, and 7 with shared GO term enrichment for chloroplast and photosynthesis functions. In addition, the anticorrelated clusters 1 and 3 overlapped in pathways resulting in the formation of organic and inorganic nitrogenous compounds, which include tetrapyrrols. Clusters 6 and 8, which showed *lhp1*-dependent upregulation, were more loosely connected by higher level terms, such as response to hormone stimulus and inorganic substance. Only cluster 8 was strongly enriched for GO terms belonging to flower development, although some of the key genes attributed to the *lhp1* phenotype such as *AG* and *AP3* were found in cluster 6.

Site II TCP Binding Motif Is Related to Reduced Expression in the *trb1-1* Mutant

We searched for enriched sequence motifs within each k-cluster using 500 nucleotide proximal promoter regions. Long *A*-tracts were enriched in all clusters but cluster 5 was also enriched for a putative *cis*-element (*AGGCAAA*), previously described as *site II* TCP binding motif (Tremousaygue et al., 2003; Welchen and Gonzalez, 2005). In combination with a minimal promoter, the *site II* motif had been shown to be necessary and sufficient to drive expression in rapidly cycling cells (Tremousaygue et al., 2003). Interestingly, the *site II* motif is often associated with *teloboxes* in promoters of genes encoding ribosomal proteins and components of the translational apparatus. *Teloboxes* (*AAACCCTA*) are related to telomeric repeats (*CCCTAAA* × *n*; *n* = *2-1000*+), which were previously shown to bind TRB1 in vitro (Schrumpfova et al., 2004; Hofr et al., 2009). The presence of *teloboxes* enhances the effect conferred by *site II* motifs but is not sufficient to drive expression from a minimal promoter on its own (Tremousaygue et al., 2003; Gaspin et al., 2010). Cluster 5 was indeed enriched for ribosomal genes, corroborating the previous link to *site II* motifs. However, *teloboxes*, although present, were not overrepresented in the corresponding promoter set, which could be due to the high incidence of *teloboxes* among all Arabidopsis promoters used as a background in the enrichment analysis (Tremousaygue et al., 2003; Gaspin et al., 2010). Cluster 5 contained the most highly expressed gene set (Figure 3A), which was expressed at lower levels in the *trb1-1* and *trb1-1 lhp1* background. Thus, within cluster 5, TRB1 binding to *teloboxes* would fit the previously described model of enhanced upregulation of *site II* containing promoters by the presence of TRB1 bound to *teloboxes*.

TRB1 Binds to Thousands of Sites

While the enrichment of *site II* motifs at genes repressed in the *trb1-1* backgrounds suggested that misregulation in cluster 5 was a direct effect, it did not explain enhanced upregulation of PcG target genes in cluster 6. We therefore performed ChIP-seq

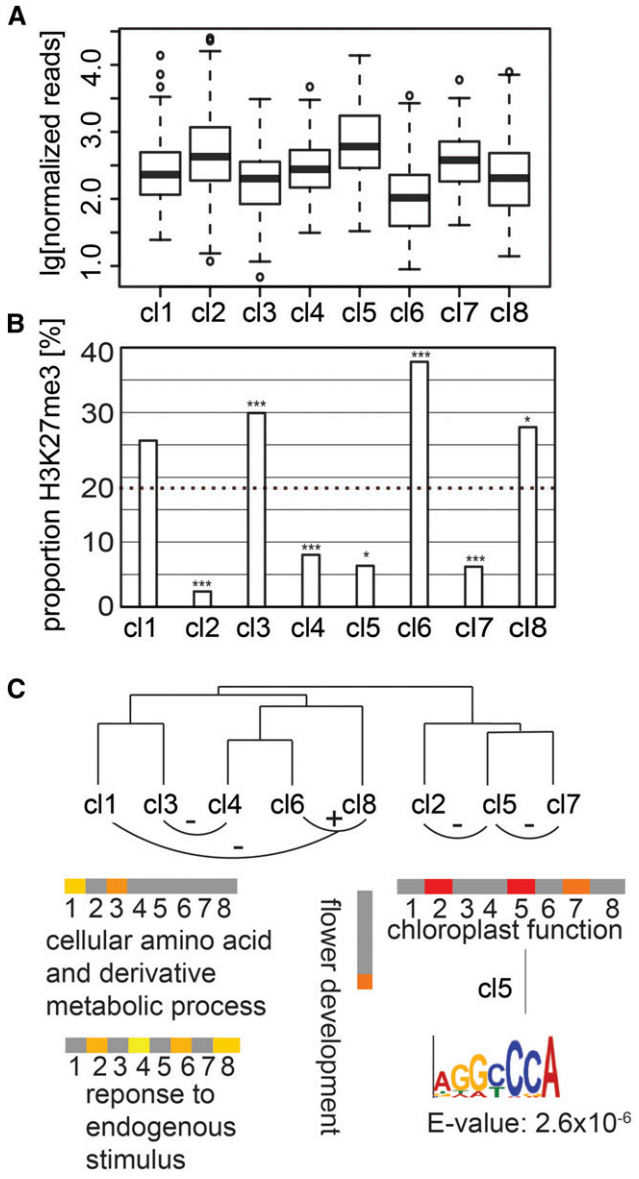

Figure 3. Analysis of Gene Clusters Affected in the *trb1* Mutant Background.

(A) Box plot showing median normalized log-transformed expression across all genes per cluster (cl). Thick horizontal lines represent the median, boxes represent the 25th to 75th percentiles, the whiskers represent the 5th and 95th percentiles, and dots indicate outliers.

(B) Proportion of H3K27me3 target genes per cluster. Genome average of H3K27me3 is indicated by dashed line. Significant deviation from genome average was tested by Fisher's exact (*P < 0.05, **P < 0.01, and ***P < 0.005).

(C) Gene clusters were further clustered according to the number of shared GO terms (dendrogram). Curved lines indicate positive (+) and negative (−) correlations between expression of the clusters. The most significant shared GO term is indicated below the tree. The pictogram indicates statistical significance of enriched GO term (yellow, lower; orange, intermediate, red, higher significance). An enriched *site II* sequence motif found in cluster 5 is indicated below.

experiments in Arabidopsis seedlings to identify direct target genes of TRB1.

ChIP-seq libraries were prepared in two biological replicates using chromatin prepared from *CaMV Pro35S:TRB1:GFP* lines in the *trb1-1* background (from now TRB1:GFP). The lines were generated by segregating the *lhp1* mutation away from a complemented TRB1:GFP *lhp1* line (Supplemental Figure 1A). TRB1:GFP significantly enriched 7825 genomic sites over a background prepared from wild-type chromatin and precipitated with the same antibodies (SICER pipeline, false discovery rate [FDR] < 0.0001; Supplemental Figure 7, Supplemental Data Set 5, and https://gbrowse.mpipz.mpg.de/cgi-bin/gbrowse/arabidopsis10_turck_public/). The overlap of target regions between biological replicates was between 73 and 80% and a majority were around 250 bp long, indicating single or closely clustered binding events (Supplemental Figure 7B).

Sequences under the TRB1 peaks were scored for enrichment and for their probability of being located at the center of enriched regions. The *telobox* was among the most significantly enriched motifs (MEME, P < 2.84.6e-61; Figure 4A; Supplemental Data Set 6 and Supplemental Figure 8). The analysis also revealed a previously undescribed related *CRACCTA* motif, now named *celobox* (DREME, P < 5.8e-96), that was even more strongly enriched at peak centers (Figure 4A). In fact, by far the most significant enrichment was detected for a shorter *telobox*-related motif (*RMCCTA*) that is included in both *telo-* and *celoboxes* (DREME, P < 1.3e-273; Figure 4A). In addition, the consensus sequence *RGCCCW*, which comprises the *site II* motif was significantly enriched, although positioned slightly off-center (Figure 4A).

To evaluate the chromatin context in which TRB1 binding sites were located, we used data from a study that classified the genome of the Arabidopsis seedling into nine distinct chromatin types based on a comprehensive analysis of genome-wide chromatin modification data (Sequeira-Mendes et al., 2014). We compared chromatin states at TRB1 binding sites to 100 permutated data sets with randomly reshuffled binding coordinates to test for significant over or underrepresentation. Chromatin states 1 and 2 are enriched for proximal promoter signatures such as H3K4me2, H3K4me3, H3 acetylation, H3K36me3, H2Bub, and H2A.Z but differ by the respective absence and presence of H3K27me3. Both states were significantly overrepresented in TRB1 peaks, while states 7, 8, and 9, corresponding to intergenic regions and heterochromatin signatures, are clearly underrepresented. Likewise, state 3 enriched in marks for elongating transcription is underrepresented (P < 0.01). State 4 is similar to state 2, but without the marks corresponding to transcription start sites (TSSs). H3K27me3 levels are high in state 4, but distal promoter regions rather than gene bodies are represented. State 4 is overrepresented among the TRB1 target regions (P < 0.01). States 5 and 6, corresponding to intergenic regions with or without H3K27me3, respectively, are neither over- nor underrepresented (Supplemental Figure 9).

We scored 6782 genes as TRB1 target genes by overlapping enriched regions with either the promoter (up to 3 kb from the ATG) or the gene body (including 250-bp downstream regions). Consistent with previous reports on the coincidence of *site II* motifs and *teloboxes* (Tremousaygue et al., 2003; Gaspin et al., 2010), we found ribosomal protein genes overrepresented among direct TRB1 target genes (Figure 4B). In addition, while *tRNA* and *snoRNA* genes were marginally enriched among the targets,

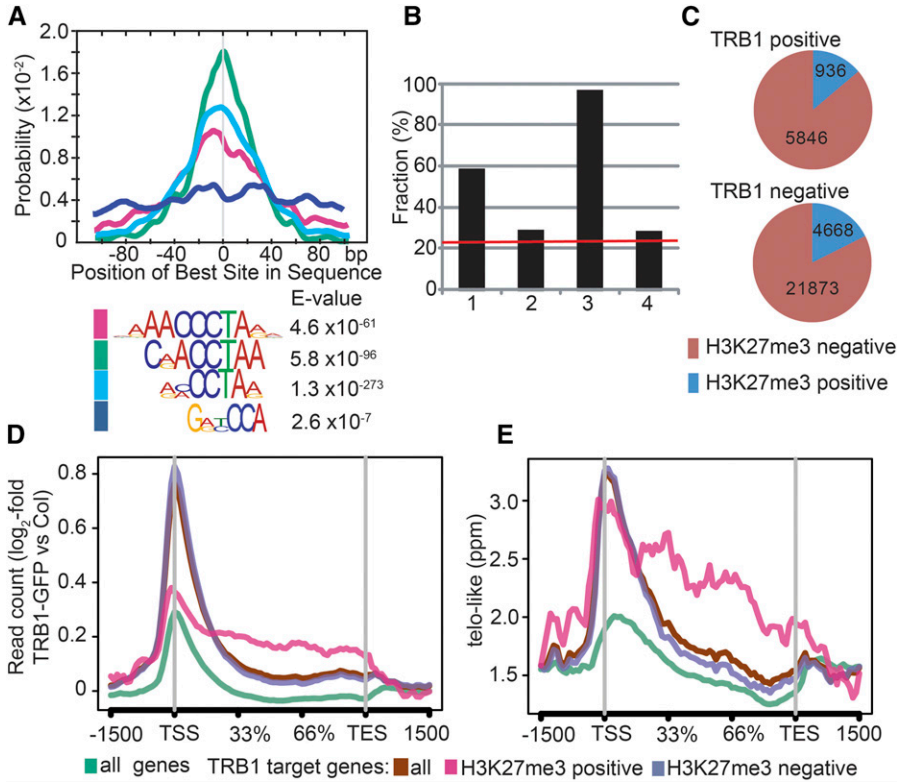

Figure 4. Analysis of TRB1 Target Sites in Seedlings.

(A) *cis*-elements enriched in TRB1 target regions. Regions enriched in TRB1:GFP compared with Col were interrogated for centrally enriched *cis*-elements by MEME-ChIP. Consensus sequences with corresponding E-values (bottom) and probabilities of occurrence around the fragment's center (top).
(B) Proportion of TRB1 targets among the genes encoding ribosomal functions. 1, Ribosomal protein; 2, tRNA; 3, intron-containing tRNA; 4, snoRNA.
(C) Proportion of H3K27me3 target (blue) and non-target (red) genes for TRB1 positive (upper pie) and negative (lower pie) genes.
(D) and **(E)** Metagene analysis of TRB1 target genes.
(D) Background-corrected TRB1:GFP ChIP-seq reads for all genes (green), all TRB1 target genes (brown), and H3K27me3 negative (purple) or positive (pink) TRB1 target genes.
(E) Frequency of *RMCCTAR* consensus for gene categories as in **(D)**. Genes are represented in relative length from TSS to transcriptional exit site (TES). Sequences 5′ and 3′ of TSS and transcriptional exit site, respectively, are scaled in base pairs.

a subset of intron-containing *tRNA* genes was strongly over-represented (Figure 4B).

Only k-cluster 1 and, as expected, cluster 5 showed an over-representation of direct TRB1 target genes (Fisher's exact test, P < 3.30e-02 and P < 6.83e-03, respectively). By contrast, cluster 6, which is H3K27me3 enriched and most affected with regard to expression in *trb1 lhp1* double mutants, was depleted in target genes, although the effect was not statistically significant. However, only 14% of TRB1 target genes were also PcG targets, which is significantly less than the expected genome-wide 20% (Fisher's exact test, P < 2.00e-08; Figure 4C).

Strikingly, the TRB1 binding pattern across target loci differed for PcG target and non-target genes. While TRB1 almost exclusively bound at the TSS of genes that were not PcG targets, it associated more evenly across gene bodies at PcG target genes (Figure 4D). Occurrence patterns of *telobox*-related motifs recapitulated this differential distribution by being particularly enriched across the gene bodies of H3K27me3-positive TRB1 target genes, while most strongly enriched at the promoters of the other genes (Figure 4E).

In conclusion, TRB1 binds preferentially to *telobox*-related motifs located at the TSS for most of its targets, while at PcG target genes, TRB1 binding spreads across gene bodies and, based on its relative enrichment in chromatin state 4, possibly also distal promoter regions. This pattern is mirrored by an increased occurrence of *telobox*-related motifs.

LHP1 Competes with TRB1 at PcG Target Genes

It seemed likely that LHP1 prevents TRB1 from binding to target sites located at PcG target genes, which would be congruent with the observation that effects on expression were only observed in the *trb1-1 lhp1* but not the *trb1-1* background. We tested this by performing ChIP-seq experiments with chromatin prepared from *TRB1:GFP lhp1* seedlings. The levels of TRB1:GFP as well as its accumulation in the nucleus and nucleolus were unaffected by the *lhp1* mutation (Supplemental Figure 10). Nevertheless, the number of target regions passing the enrichment level was significantly increased in the *lhp1* background, although H3K27me3

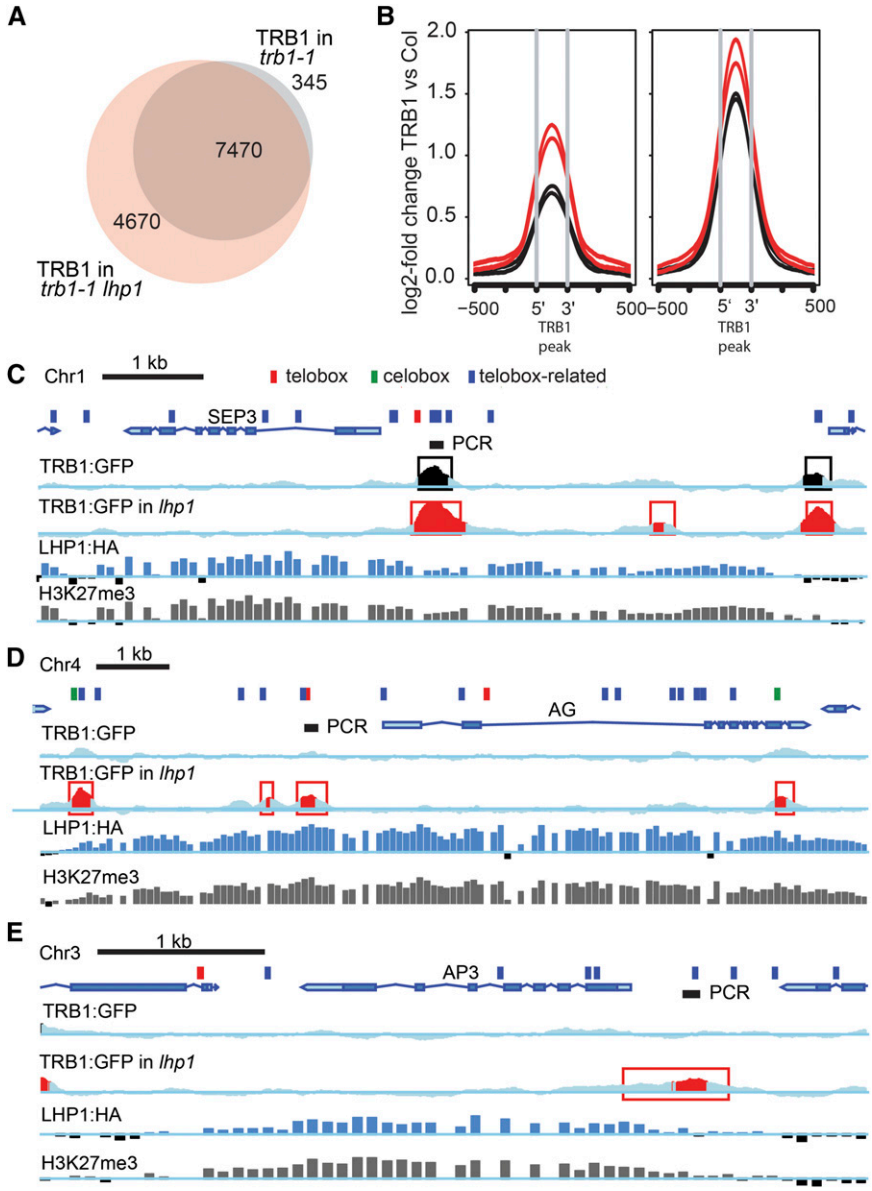

Figure 5. Comparison of TRB1 Target Sites in the Wild Type and *lhp1*.

(A) Venn diagram showing the number of regions associated with TRB1:GFP (gray) and TRB1:GFP *lhp1* (red).

(B) Read depth (corrected for read depth at control precipitation) across all fragments enriched only in TRB1:GFP *lhp1* (left panel) or in both genetic backgrounds (right panel). ChIP-seq data are based on two biological replicates of *TRB1:GFP* (black lines) and *TRB1:GFP lhp1* (red lines). Enriched fragments are displayed between gray lines on a fraction of length scale and flanking regions on a base pair scale.

(C) Overview of the *SEP3* locus. Top panels show gene models with exons and introns illustrated by boxes and lines, respectively. Untranslated regions are depicted by lighter blue fill color; direction of the coding strand is indicated by the arrow. Location of *telobox*-related, *telobox*, and *celobox* motifs are indicated by blue, red, and green boxes, respectively. Middle panels show coverage of TRB1:GFP and TRB1:GFP *lhp1* corrected by coverage from Col control precipitation. Values more than 50 reads over background are indicated in black for TRB1:GFP and red for TRB1:GFP *lhp1*. Black and red boxes indicate location of fragments indicates significantly enriched by SICER (FDR < 0.0001). Two bottom panels show ChIP-chip enrichment of LHP1:HA and H3K27me3 from our previously published data (Dong et al., 2012; Engelhorn et al., 2012).

(D) Overview of *AG* locus; colors and symbols same as for **(C)**.

(E) Overview of the AP3 locus; colors and symbols same as for **(C)**.

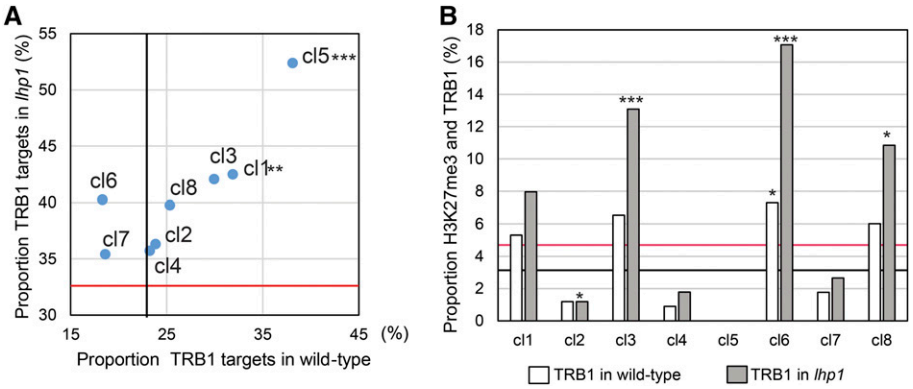

Figure 6. Comparison of TRB1 Target Genes within Transcriptional Cluster Groups between the Wild Type and *lhp1*.

(A) Scatterplot of proportion of TRB target genes per transcriptional cluster for the wild type and *lhp1* among genes misregulated in *trb1-1*, *lhp1*, and *trb1-1 lhp1*. Genome-wide proportion for the wild type and *lhp1* is indicated by a black and a red line, respectively. Statistical difference from expected indicated by asterisks (Fisher's exact test, *P < 0.05, **P < 0.01, and ***P < 0.005).

(B) Proportion of genes that are both TRB1 and H3K27me3 positive in the wild type and *lhp1*. Genome-wide proportion indicated by a black and a red line for the wild type and *lhp1*, respectively. Significant deviation from genome average was tested by Fisher's exact (*P < 0.05, **P < 0.01, and ***P < 0.005).

target genes were still underrepresented (Fisher's exact test P < 2.20e-16; Figure 5A; Supplemental Data Set 7). Increased binding of TRB1 in *lhp1* was quantitative more than qualitative, since average signals at target sites were slightly higher for regions already enriched in the wild type, while *lhp1* unique regions often failed to pass the stringent significance threshold for enrichment in the wild type (Figure 5B). Increased TRB1 binding was detected at both H3K27me3-positive and -negative binding sites (Supplemental Figure 11). *AG*, *AP3* (cluster 6), and *SEP3* (cluster 8) were among the TRB1:GFP *lhp1* target genes, but only *SEP3* was already scored as positive in TRB1:GFP (Figures 5C and 5D; https://gbrowse.mpipz.mpg.de/cgi-bin/gbrowse/arabidopsis10_turck_public/). Likewise, TRB1 bound the *FT* (cluster 8) promoter regions in both backgrounds (Supplemental Figure 12). We confirmed these results by ChIP-qPCR for *AG*, *AP3*, *SEP3*, and *FT* (Supplemental Figure 12).

In general, the increase in the number of target genes was proportional to the genome average for all transcriptional clusters, with the notable exception of cluster 6 that went from underrepresented in TRB1 targets in the wild type to enriched in *lhp1* compared with the genome-wide distribution, although neither value was statistically significant (Figure 6A). However, this relative enrichment became highly relevant if targeting by both H3K27me3 and TRB1 was considered (Figure 6B).

In conclusion, LHP1 prevents binding of TRB1 at many target sites, which are not all scored as PcG-positive genes. Increased binding of TRB1 to PcG target genes occurs in particular at transcriptional cluster 6, which is the most upregulated in the *trb1-1 lhp1* double mutant.

DISCUSSION

A Model for the Role of TRB1 in Transcriptional Regulation

Here, we report that TRB1 can affect the expression of direct target genes by binding to *telobox*-related elements. The direction in which expression is altered in comparison to relevant controls cannot be predicted, although the following tendencies were detected. First, a functionally correlated set of highly expressed TRB1 target genes is expressed at lower levels in the absence of TRB1 in both the wild type and *lhp1* mutant background. A second group, corresponding predominantly to PcG target genes showing TRB1 binding only in the *lhp1* mutant background, shows strongly enhanced induction in *trb1-1 lhp1* compared with *lhp1*. At these loci, TRB1 seems to implement a second layer of repression.

Several models can explain our findings (Figure 7). First, it seems likely, based on previous data showing the synergistic role of *teloboxes* and *site II* motifs (Tremousaygue et al., 2003), that TRB1 binding to *teloboxes* per se is neutral to transcription but assists in the activation function realized by TCP factors binding to *site II*. It has been reported that transcription factor binding sites need to cluster, as binding of a single one would not be sufficient to displace nucleosomes from cognate binding sites (Mirny, 2010; Moyle-Heyrman et al., 2011). In such a scenario, the presence of TRB1 would assist in liberating the binding site for TCPs or other transcription factors that could either be transcriptional activators or repressors. In a more elaborate model, TRB1 binding would not be quite neutral but lead to the recruitment of chromatin remodeling factors that promote binding of other factors. The role of TRB1 at PcG target genes could be explained by the participation of chromatin remodelers because these can participate in maintaining a less permissive chromatin structure. Such ambivalent roles as activators and repressors have been reported for the complex around the CHD4-type ATPase PICKLE (PKL), which reportedly antagonizes PcG-mediated repression (Aichinger et al., 2011), but at the same time helps to maintain H3K27me3 at several direct target genes (Zhang et al., 2012). Likewise, the SWI/SNF2-type ATPase BRAHMA is required to repress the PcG target gene *FLC* (Farrona et al., 2011a) while antagonizing H3K27me3 deposition at many of its direct targets (Li et al., 2015). As for the last example, the SWR1 complex that exchanges canonical histone H2A with H2A.Z is thought to facilitate both transcriptional activation and repression by creating boundaries for transcription

factor binding sites at TSS (Kumar and Wigge, 2010; Farrona et al., 2011a).

Telobox-Related Elements and Transcription in an Evolutionary Context

The presence of *cis*-elements related to telomere repeats is conserved in plants, yeast, and human (Ruiz-Herrera et al., 2008; Vaquero-Sedas and Vega-Palas, 2011). It has been speculated that these evolve rapidly from interstitial telomere repeats, which form by the invasion of chromosomal ends into extratelomeric regions (Gaspin et al., 2010). In any case, it seems that the connection of telomere-derived *cis*-elements and cognate transcription factors with genes encoding proteins involved in primary cellular functions is an ancient one, although the outcome on gene regulation can be quite different from the one reported in plants (Ye et al., 2014). For example, the yeast Myb-related factor Rap1 binds at telomeric and extratelomeric sites, where it can contribute to either up- or downregulation of target genes. During senescence, the shortening of telomeres releases more Rap1 protein to bind at extratelomeric sites, leading to downregulation of genes encoding core histones and the translational apparatus, while supporting upregulation of other target genes responsive to senescence (Platt et al., 2013). In mammals, the TELOMERE REPEAT FACTOR2, a homolog of plant TRBs, binds to extratelomeric sites, which can contribute to either up- or downregulation of target genes (Yang et al., 2011).

cis-Elements at PcG Target Genes

At PcG target genes, TSS sites were present at a normal proportion but were not as likely bound by TRB1 as were other target genes. By contrast, binding across the gene body was increased, as was the number of *telobox*-related motifs. It is possible that the increased number of motifs is a means to compensate for the more restricted access due to chromatin compaction at H3K27me3-positive genes. It is possible that these sites become accessible during transcription, which may occur at a low rate due to spontaneous chromatin state switching (Angel et al., 2011; Satake and Iwasa, 2012). In this case, the presence of TRB1 as a second layer of repression is important to avoid leaky expression of target genes.

Our study is not the first that links the PcG pathway to *telobox* motifs. A genome-wide survey of binding sites for the PRC2 component FERTILIZATION INDEPENDENT ENDOSPERM (FIE) reported an enrichment of *teloboxes* as well as *GAGA* and *GAAGAA* repeat motifs at FIE-enriched peaks (Deng et al., 2013). Furthermore, a recent study reports an overrepresentation of teloboxes particularly at those PcG target genes that show strongly reduced H3K27me3 levels in the *clf* mutant background (Wang et al., 2016). A link between the *GAGA*-motif and PcG recruitment was suggested by showing that *GAGA* binding proteins, such as BPC6, could bind to both *GAGA*-motifs and LHP1 in vitro (Hecker et al., 2015). In the case of TRBs, we think it unlikely that they act as recruiters of PcG components due to their extensive binding at PcG non-target genes.

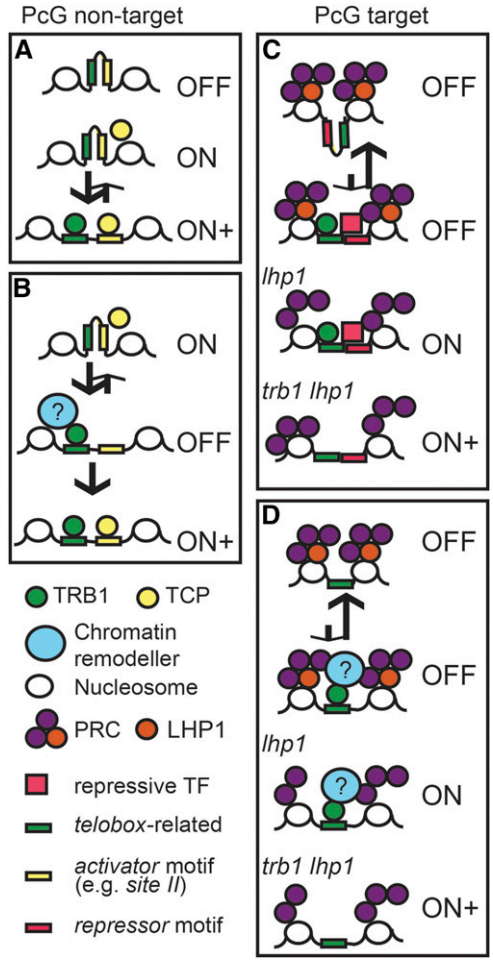

Figure 7. Working Model for Transcriptional Regulation by TRB1.

(A) and **(B)** Model for highly expressed genes in cluster 5.

(A) TRB1 binds to *telobox*-like motifs, thereby facilitating the binding of TCP factors to *site II* motifs. Genes are highly expressed in the absence of TRB (ON), while the presence of both factors helps to express genes at very high levels (ON+), but the presence of TCP is a dominant requirement for expression (OFF). In principle, the mechanisms could also apply to coregulation by other *cis*-elements and cofactors, which could also be repressors.

(B) As in **(A)** but TRB1 recruits chromatin remodelers to assist binding of TCP factors or support their downstream effect on transcription activation.

(C) and **(D)** TRB1 action at PcG target genes, showing enhanced upregulation in the double mutant.

(C) TRB1 basically functions as in **(A)** but facilitates the action of a repressor that participates in downregulation but has no dominant effect. In the wild type, there is an equilibrium between LHP1-dependent and TRB1-dependent repression and targets are always repressed (OFF). In *lhp1* plants, a repressor can bind with the help of TRB1 and attenuate upregulation (ON). In *trb1 lhp1* double mutants, attenuation is lost, leading to enhanced expression (ON+).

(D) TRB1 acts similar as in **(B)** by recruiting a chromatin remodeler. The remodeler maintains a more closed chromatin conformation but can only partially compensate for the lack of LHP1. Genes are not expressed in the wild type and *trb1* single mutants (OFF), are induced in *lhp1* mutants (ON), and are hyperinduced in *trb1 lhp1* double mutants (ON+).

Conclusion

We find that TRBs are novel transcriptional coregulators that potentially impact thousands of genes, a number of which are more commonly associated with chromatin regulatory complexes than sequence-specific transcription factors, which show more restricted binding. TRBs seem to assist rather than define target gene regulation. In consequence, their presence does not predict the direction of transcriptional regulation, which is defined by the presence of other *cis*-elements or chromatin components. At PcG target genes, TRB1 binding is generally reduced, while the number of cognate binding sites increases. It seems that PcG complexes rely on TRBs as second-layer repressive backup.

METHODS

Mutagenesis, Mutant Screening, and Cloning

Mutagenesis, screening for enhanced *lhp1* genotypes, and cloning of causal mutations was as previously described (Hartwig et al., 2012). Briefly, 200 mg of *lhp1-3* (Larsson et al., 1998) mutant seeds was incubated in 100 mL of 30 mM EMS for 12 h after pretreatment in 0.1% KCl solution at 4°C for 14 h. Mutagenized seeds were washed with distilled water and incubated in 100 mL sodium thiosulfate (100 mM, 15 min) followed by three washing steps in 500 mL of deionized water 30 min prior to transfer to soil.

For mutant screening, M2 mutant families were grown in soil in a greenhouse at 22°C in short-day conditions (8 h light/16 h dark) and scored visually for an enhancement of the early flowering and reduced size *lhp1* mutant phenotype. M3 seeds of mutants were grown in growth chambers for confirmation of the phenotype (60% humidity, 12 h; 16°C light/12 h dark; 14°C cycles).

For cloning of the causative gene, phenotypically confirmed M3 mutants were backcrossed twice to *lhp1-3* to generate a BC2F2 population of 1000 individuals. Leaf material from plants with a mutant phenotype (*trb1 lhp1*, $n = 240$; *trb3 lhp1*, $n = 295$) was pooled for DNA preparation (DNeasy Plant Maxi Kit; Qiagen; according to the manufacturer's instructions) and NGS library preparation (Illumina True-seq). On the IlluminaHiSeq platforms 60E6 and 80E6, 50-bp reads were generated for *trb1 lhp1* and *trb3 lhp1*, respectively, resulting in genome coverage of 37- and 50-fold. Using the fast isogenic mapping pipeline (Hartwig et al., 2012), four linked possibly homozygous candidate single nucleotide polymorphisms resulting in nonsynonymous codons were identified per genotype. Of these, only *trb1-1* and *trb3-1* alleles represented homologs.

Plant Materials

The EMS-induced *lhp1-3* allele in the Col background has been described previously as *terminal flower 2-1* (*tfl2-1*) but has also been referred to as *tfl2-2* (Kotake et al., 2003). The *trb1-2* and *trb3-2* alleles were obtained from the SALK T-DNA insertion line collection (SALK_001540 and SALK_134641, respectively). The *ku70*, *tert* (−/+), and *tert* (G5) mutants were provided by Karel Riha at the Gregor Mendel Institute of Molecular Plant Biology, Austria.

Cultivation Conditions

For qRT-PCR/RNA-seq and ChIP-PCR/ChIP-seq, seeds of corresponding Col-0 and mutants were sterilized in 75% ethanol and sown on GM medium. Materials from 10-d-old seedlings grown in Percival growth chambers at 22°C in long days (16 h light/8 h dark) were collected. For phenotypic analysis, seeds were sown on soil and transferred to long days after stratification (4°C, 3 d). Flowering time was determined by counting the number of rosette and cauline leaves of the main shoot. Plant size was measured as longest diameter at bolting. Test for statistical significance was performed by one-way ANOVA followed by a Tukey HSD correction for multiple comparisons and by a Student's *t* test for comparisons of two groups.

Plasmid Construction and Generation of Transgenic Plants

Full-length *LHP1*, *TRB1*, and *TRB3* cDNAs without stop codons were amplified from Col-0 cDNA. Genomic sequence (2.0 kb upstream of ATG, full gene body, and 1.5 kb downstream of stop codon) and promoter sequence (2.0 kb upstream of ATG) of *TRB1* and *TRB3* were amplified from genomic DNA of Col-0. Oligonucleotide primers were Gateway (GW) compatible and are indicated in Supplemental Table 2. Fragments were introduced into the pDONR207 vector (Invitrogen) and then to *Agrobacterium tumefaciens* binary vectors by GW recombination reactions according to the manufacturer's instructions. Coding sequences of *LHP1*, *TRB1*, and *TRB3* were recombined into Pro35S:GW:GFP-pAM or Pro35S:GW:tagRFP-pCZN654 (a gift from Richard Immink) to create C-terminal fusions to GFP and RFP under the control of the CaMV 35S promoter; genomic *TRB1* and *TRB3* sequences were introduced into pGD2B (a gift from Hailong An) to allow expression under the control of their native regulator regions. *TRB1* and *TRB3* promoter sequence were introduced into GW:GUS-pGREEN (Adrian et al., 2010) to drive expression of the GUS reporter gene. Vector backbones are provided in GenBank format (Supplemental Data Set 8). Transgenic plants were generated by Agrobacterium-mediated transfer using the floral dip method (Clough and Bent, 1998). TRB1:GFP expression constructs were generated in the *trb1-1 lhp1* mutant background from which the *lhp1-3* allele was subsequently removed by crossing to Col-0 wild type.

Fluorescence Microscopy

To determine the cellular localization of *LHP1*, *TRB1*, and *TRB3*, fusions to *GFP* and *tagRFP* were transiently expressed in 3-week-old *Nicotiana benthamiana* (tobacco) plants by Agrobacterium infiltration. Briefly, Agrobacterium strains carrying plasmids encoding fusion proteins and the *p19* silencing suppressor were grown overnight at 28°C in 10 mL YEP medium plus selective antibiotics and then collected and resuspended in infiltration buffer (10 mM $MgCl_2$, 10 mM MES, pH 5.6, and 150 μg/mL acetosyringone). Resupended bacteria were incubated at 28°C for 3 h in the dark and infiltrated to the lower surface of tobacco leaves with a needle-free syringe. Cellular localization of fusion proteins was examined under a LSM 700 confocal laser scanning microscopy (Carl Zeiss). Comparative fluorescence intensity scanning was performed by pixel density analysis using ImageJ software.

Terminal Restriction Fragment Analysis

DNA was extracted from pooled (10 to 20) 10-d-old seedlings and 31-d-old single plants with the DNeasy Plant Mini Kit (Qiagen). DNA (3 μg) was digested with restriction endonuclease Tru1I (Fermentas) at 42°C overnight. Digested DNA was electrophoresed on an agarose gel and blotted to a polyvinylidene fluoride membrane. $(T_3AG_3)_4$ oligonucleotide was end-labeled by ^{32}P and was used as hybridization probe for DNA gel blotting.

GUS Staining

For GUS staining, 10-d-old seedlings were incubated for 30 min in 90% (v/v) acetone on ice, rinsed with 50 mM sodium phosphate buffer, pH 7.0, and incubated overnight at 37°C in staining solution (0.5 mg/mL X-Gluc, 50 mM sodium phosphate buffer, pH 7.0, 0.5 mM potassium ferrocyanide, 0.5 mM potassium ferricyanide, and 0.1% [v/v] Triton X-100). After staining, samples were washed with 50 mM sodium phosphate buffer, pH 7.0, and cleared in 70% (v/v) ethanol. The GUS staining results were visualized under a light stereomicroscope (MZ 16 FA; Leica).

RNA Isolation, Quantitative RT-PCR, and RNA-Seq

Total RNA was extracted using the RNeasy Mini Kit (Qiagen) according to the manufacturer's instructions. Total RNA (5 µg) was treated with DNaseI (DNA-free kit; Ambion). For RT-PCR, cDNA was generated at 42°C for 2 h using Superscript II reverse transcriptase and T18 oligonucleotide for priming (Life Technologies). Expression of *TRB1* and *TRB3* of T-DNA lines was measured by PCR using *PP2A* as control. For quantitative RT-PCR, experiments were performed in a Bio-Rad iQ5 apparatus using a home-made Eva-GREEN amplification cocktail (80 mM KCl, 20 mM Tris-HCl; pH 8.0, 5 mM $MgCl_2$, 0.4 mM deoxynucleotide triphosphate, 400 nM forward and reverse oligonucleotide primer, 1× EVAGreeen dye [Biotium], and 0.1 units/µL Taq polymerase) for detection. Quantification was performed using the relative -ΔΔCT method using *PP2A* as reference. Oligonucleotide primers are indicated in Supplemental Table 2. For RNA-seq, material was collected from three independent biological replicates, and DNA-free total RNA was generated as described above. Illumina True-seq library preparation was performed from DNA-free total RNA (3 µg) by the Max Planck Genome Centre in Cologne. Quality trimmed single-end RNA-seq reads were mapped to the Arabidopsis TAIR10 annotation using the CLC genomics workbench (parameters for quality trimming: removal of reads with ambiguous nucleotides >2, quality score <0.05, length <80 nucleotides; parameters for mapping: mismatches <3). Read per kilobase of exon models (RPKM) were calculated from 8.3e6 – 11.4e6 mapped reads per library. RPKM values were scaled to fit the medians of each library and differential expression determined using Baggerley's weighted Z-test with FDR correction as implemented by the CLC genomics workbench (threshold FDR < 0.05, fold change > 2). Transcriptional cluster analysis was performed using the Cluster3.0 software package after centering average RPKM values per gene to the median value across all samples (de Hoon et al., 2004). After empirical evaluation, k = 8 was selected for k-median clustering using Eucledian distance. Cluster results were visualized using Java TreeView (Saldanha, 2004). GO analysis was performed using the AgriGO Web tool (Du et al., 2010). Enriched GO terms were compared between k-clusters using AgriGO compare.

ChIP and ChIP-Seq

ChIP experiments were performed as previously described (Reimer and Turck, 2010). Chromatin was extracted from 10-d-old whole seedlings (1 to 3 g). GFP (Abcam; Ab290) and H3K27me3 (Millipore; 07-449) antibodies were used for chromatin immunoprecipitation. For ChIP-PCR, amplification was performed in a Bio-Rad iQ5 apparatus using a home-made Eva-GREEN amplification cocktail (80 mM KCl, 20 mM Tris-HCl, pH 8.0, 5 mM $MgCl_2$, 0.4 mM deoxynucleotide triphosphate, 400 nM forward and reverse oligonucleotide primer, 1× EVAGreeen dye [Biotium], and 0.1 units/µL Taq polymerase) for detection or Bio-Rad SYBR Green master mix. TRB1:GFP binding and H3K27me3 enrichment were normalized to input DNA prepared from a reverse cross-linked aliquot of each chromatin preparation. Quantitative PCR data are shown as the means of three technical replicates from a representative experiment from at least two biological replicates. Primers used for ChIP-PCR are shown in Supplemental Table 2. For ChIP-seq, two immunoprecipitations from independent biological replicates were processed for NGS library preparation. All libraries were prepared by the Ovation Ultralow Library Systems (NuGEN) following the manufacturer's instructions using 80% of a typical ChIP as starting material. After amplification for 16 PCR cycles, DNA of a size range of between 200 and 300 bp was purified from an agarose gel. Amplification was confirmed by testing an aliquot of the library before and after amplification by quantitative PCR. Sequencing was performed as single-end 100-nucleotide reads on an Illumina HiSeq by the Max Planck Genome Centre in Cologne. ChIP-seq reads were mapped to the TAIR10 assembly of *Arabidopsis thaliana* using the CLC genomics workbench. To identify TRB1 target regions, reads with a number of mismatches of >2 and more than one mapping position were discarded. Only one of two or more identical reads was kept for further analysis, resulting in between 12.8e6 and 28.0e6 mapped reads per sample. Enriched regions were determined from each sample by SICER (Zang et al., 2009) using libraries prepared from Col anti-GFP mock ChIP as background, windows of 80 bp, and a FDR < 0.0001 as threshold. Overlapping and directly adjacent enriched windows were merged to enriched regions. For annotation to target genes, the annotatePeaks.pl function of the Homer suite was used (Heinz et al., 2010). A custom annotation file was prepared based on the Arabidopsis TAIR10 annotation that allowed assigning enriched regions first to TSS and transcriptional exit sites ±250 bp, then to gene body regions, then to 1-kb promoter regions, and last to 3-kb promoter regions. Each fragment was assigned to only one gene. For detection of H3K27me3-enriched target regions, mapping was performed as above except that reads with more than one mapping position were randomly distributed among mapping sites. Enriched regions were detected by SICER as described above except that window size = 300 bp and FDR < 0.01 were used and the background was determined based on pooled input reads from four independent libraries prepared from reverse cross-linked chromatin. Enriched windows were merged to enriched regions if their distance was below 600 bp. Finally, enriched regions were intersected between replicates using bedtools (Quinlan and Hall, 2010) and the intersections used for further analysis. Genes were annotated as H3K27me3 positive if at least 80% of their gene body overlapped with a H3K27me3-positive region. Read traces for gbrowse were produced by randomly selecting 11e6 and 12e6 mapped reads from each TRB1 and H2K27me3 sample, respectively, extending the reads to 500 bp and calculating read depth per genomic position using bedtools (Quinlan and Hall, 2010). Coverage depth from two biological replicates was summarized to visualize averages using bedtools.

Motif Enrichment and Metagene Analysis

Enriched motifs in TRB1 target regions were identified using the MEME-ChIP Web tool (Machanick and Bailey, 2011). For region intersection and sequence extraction, the bedtools suite (Quinlan and Hall, 2010) was used. For metagene analysis, the TAIR10 assembly was annotated for enriched motifs using EMBOSS function fuzznuc (Rice et al., 2000). Metagene analysis was performed using ngs.plot.r (Shen et al., 2014). For this purpose, annotation data were converted to the binary.bam file format using custom scripts and bedtools.

Accession Numbers

Read data for RNA-seq and ChIP-seq experiments are accessible at EBI under accession code ERA422470. Processed ChIP-seq data can be visualized at the following public gbrowse link: https://gbrowse.mpipz.mpg.de/cgi-bin/gbrowse/arabidopsis10_turck_public/. Gene annotation data from this article can be found in the Arabidopsis Genome Initiative or GenBank/EMBL databases under the following accession numbers: TRB1 (AT1G49950), TRB3 (AT3G49850), LHP1 (AT5G17690), AG (AT4G18960), SEP3 (AT1G24260), AP3 (AT3G54340), FT (At1g65480), and PP2A (AT1G13320).

Supplemental Data

Supplemental Figure 1. Confirmation of mutant mapping results.

Supplemental Figure 2. Phylogenetic analysis of single-myb-Histone1/5 domain proteins in plants.

Supplemental Figure 3. Histochemical detection of GUS activity for TRB1 or TRB3.

Supplemental Figure 4. Representative comparative fluorescence profile of coexpressed TRB1 and TRB3 with LHP1 in tobacco cells.

Supplemental Figure 5. Telomere length in PcG pathway mutants.

Supplemental Figure 6. Quantitative RT-PCR analysis to confirm expression levels of TRB1 target genes in *lhp1-3* and *trb1-1 lhp1-3* background.

Supplemental Figure 7. Replicate ChIP-seq analysis of TRB1 target regions.

Supplemental Figure 8. Full analysis of *cis*-elements enriched under TRB1 ChIP-seq enriched regions in wild-type and *lhp1* backgrounds.

Supplemental Figure 9. Overlap of TRB1 binding with chromatin topologies.

Supplemental Figure 10. TRB1-GFP localization and level in wild-type and *lhp1* backgrounds.

Supplemental Figure 11. Differences in TRB1 binding strength at binding sites in wild-type and *lhp1* backgrounds.

Supplemental Figure 12. TRB1 binding at FT and ChIP-PCR confirmation of results for *AP3*, *SEP3*, *AG*, and *FT*.

Supplemental Table 1. Table of SNPs identified by isogenic mapping-by-sequencing.

Supplemental Table 2. List of oligonucleotides used in this study.

Supplemental Data Set 1. Sequence alignment in fasta format.

Supplemental Data Set 2. Comprehensive table of RNA-seq results.

Supplemental Data Set 3. Summary table of RNA-seq and ChIP-seq results for differentially expressed genes.

Supplemental Data Set 4. Summary of GO term enrichment analysis, ready for visualization with AgriGO custom compare tool.

Supplemental Data Set 5. Table of genomic fragments bound by TRB1:GFP in both replicates prepared from the *trb1-1* background and annotation of target genes.

Supplemental Data Set 6. Position weight matrices for *cis*-elements enriched under TRB1 and TRB1 *lhp1* ChIP-seq peaks.

Supplemental Data Set 7. Table of genomic fragments bound by TRB1:GFP in both replicates prepared from the *trb1-1 lhp1* background and annotation of target genes.

Supplemental Data Set 8. Plasmid backbones in GenBank format.

ACKNOWLEDGMENTS

We thank Petra Taenzler for excellent technical help. We also thank Karel Riha and Elisa Derboven (Gregor Mendel Institute of Molecular Plant Biology, Austria) for providing *ku70*, *tert* (−/+), and *tert* (G5) mutant seeds and technical advice, Richard Immink and Hailong An for providing Pro35S:GW:tagRFP-pCZN654 and pGDB2 vectors, respectively, and George Coupland for critical reading of the manuscript. We thank the Max Planck Society for funding.

AUTHOR CONTRIBUTIONS

Y.Z. carried out all experiments except for the mutant identification and mapping, which was done by B.H. G.V.J. and K.S. performed the isogenic mutant mapping analysis. F.T. analyzed ChIP-seq and RNA-seq data. Y.Z. and F.T. planned the experiments and wrote the article.

Received September 8, 2015; revised November 11, 2015; accepted December 25, 2015; published December 31, 2015.

REFERENCES

Adrian, J., Farrona, S., Reimer, J.J., Albani, M.C., Coupland, G., and Turck, F. (2010). cis-Regulatory elements and chromatin state coordinately control temporal and spatial expression of FLOWERING LOCUS T in Arabidopsis. Plant Cell **22:** 1425–1440.

Aichinger, E., Villar, C.B.R., Di Mambro, R., Sabatini, S., and Köhler, C. (2011). The CHD3 chromatin remodeler PICKLE and polycomb group proteins antagonistically regulate meristem activity in the Arabidopsis root. Plant Cell **23:** 1047–1060.

Angel, A., Song, J., Dean, C., and Howard, M. (2011). A Polycomb-based switch underlying quantitative epigenetic memory. Nature **476:** 105–108.

Beh, L.Y., Colwell, L.J., and Francis, N.J. (2012). A core subunit of Polycomb repressive complex 1 is broadly conserved in function but not primary sequence. Proc. Natl. Acad. Sci. USA **109:** E1063–E1071.

Bratzel, F., López-Torrejón, G., Koch, M., Del Pozo, J.C., and Calonje, M. (2010). Keeping cell identity in Arabidopsis requires PRC1 RING-finger homologs that catalyze H2A monoubiquitination. Curr. Biol. **20:** 1853–1859.

Calonje, M. (2014). PRC1 marks the difference in plant PcG repression. Mol. Plant **7:** 459–471.

Calonje, M., Sanchez, R., Chen, L., and Sung, Z.R. (2008). EMBRYONIC FLOWER1 participates in polycomb group-mediated AG gene silencing in Arabidopsis. Plant Cell **20:** 277–291.

Chanvivattana, Y., Bishopp, A., Schubert, D., Stock, C., Moon, Y.H., Sung, Z.R., and Goodrich, J. (2004). Interaction of Polycomb-group proteins controlling flowering in Arabidopsis. Development **131:** 5263–5276.

Chen, D., Molitor, A., Liu, C., and Shen, W.H. (2010). The Arabidopsis PRC1-like ring-finger proteins are necessary for repression of embryonic traits during vegetative growth. Cell Res. **20:** 1332–1344.

Clough, S.J., and Bent, A.F. (1998). Floral dip: a simplified method for Agrobacterium-mediated transformation of *Arabidopsis thaliana*. Plant J. **16:** 735–743.

Cui, H., and Benfey, P.N. (2009). Interplay between SCARECROW, GA and LIKE HETEROCHROMATIN PROTEIN 1 in ground tissue patterning in the Arabidopsis root. Plant J. **58:** 1016–1027.

de Hoon, M.J., Imoto, S., Nolan, J., and Miyano, S. (2004). Open source clustering software. Bioinformatics **20:** 1453–1454.

Deng, W., Buzas, D.M., Ying, H., Robertson, M., Taylor, J., Peacock, W.J., Dennis, E.S., and Helliwell, C. (2013). Arabidopsis Polycomb Repressive Complex 2 binding sites contain putative GAGA factor binding motifs within coding regions of genes. BMC Genomics **14:** 593.

Derkacheva, M., and Hennig, L. (2014). Variations on a theme: Polycomb group proteins in plants. J. Exp. Bot. **65:** 2769–2784.

Derkacheva, M., Steinbach, Y., Wildhaber, T., Mozgová, I., Mahrez, W., Nanni, P., Bischof, S., Gruissem, W., and Hennig, L. (2013). Arabidopsis MSI1 connects LHP1 to PRC2 complexes. EMBO J. **32:** 2073–2085.

Dong, X., Reimer, J., Göbel, U., Engelhorn, J., He, F., Schoof, H., and Turck, F. (2012). Natural variation of H3K27me3 distribution between two Arabidopsis accessions and its association with flanking transposable elements. Genome Biol. **13:** R117.

Du, Z., Zhou, X., Ling, Y., Zhang, Z., and Su, Z. (2010). agriGO: a GO analysis toolkit for the agricultural community. Nucleic Acids Res. **38:** W64–W70.

Engelhorn, J., Reimer, J.J., Leuz, I., Göbel, U., Huettel, B., Farrona, S., and Turck, F. (2012). Development-related PcG target in the apex 4 controls leaf margin architecture in *Arabidopsis thaliana*. Development **139:** 2566–2575.

Exner, V., Aichinger, E., Shu, H., Wildhaber, T., Alfarano, P., Caflisch, A., Gruissem, W., Köhler, C., and Hennig, L. (2009). The chromodomain of LIKE HETEROCHROMATIN PROTEIN 1 is

essential for H3K27me3 binding and function during Arabidopsis development. PLoS One **4:** e5335.

Farrona, S., Hurtado, L., March-Díaz, R., Schmitz, R.J., Florencio, F.J., Turck, F., Amasino, R.M., and Reyes, J.C. (2011a). Brahma is required for proper expression of the floral repressor FLC in Arabidopsis. PLoS One **6:** e17997.

Farrona, S., Thorpe, F.L., Engelhorn, J., Adrian, J., Dong, X., Sarid-Krebs, L., Goodrich, J., and Turck, F. (2011b). Tissue-specific expression of FLOWERING LOCUS T in Arabidopsis is maintained independently of polycomb group protein repression. Plant Cell **23:** 3204–3214.

Gaspin, C., Rami, J.F., and Lescure, B. (2010). Distribution of short interstitial telomere motifs in two plant genomes: putative origin and function. BMC Plant Biol. **10:** 283.

Gaudin, V., Libault, M., Pouteau, S., Juul, T., Zhao, G., Lefebvre, D., and Grandjean, O. (2001). Mutations in LIKE HETEROCHROMATIN PROTEIN 1 affect flowering time and plant architecture in Arabidopsis. Development **128:** 4847–4858.

Hartwig, B., James, G.V., Konrad, K., Schneeberger, K., and Turck, F. (2012). Fast isogenic mapping-by-sequencing of ethyl methanesulfonate-induced mutant bulks. Plant Physiol. **160:** 591–600.

Hecker, A., Brand, L.H., Peter, S., Simoncello, N., Kilian, J., Harter, K., Gaudin, V., and Wanke, D. (2015). The Arabidopsis GAGA-binding factor BASIC PENTACYSTEINE6 recruits the POLYCOMB-REPRESSIVE COMPLEX1 component LIKE HETEROCHROMATIN PROTEIN1 to GAGA DNA motifs. Plant Physiol. **168:** 1013–1024.

Heinz, S., Benner, C., Spann, N., Bertolino, E., Lin, Y.C., Laslo, P., Cheng, J.X., Murre, C., Singh, H., and Glass, C.K. (2010). Simple combinations of lineage-determining transcription factors prime cis-regulatory elements required for macrophage and B cell identities. Mol. Cell **38:** 576–589.

Hofr, C., Sultesova, P., Zimmermann, M., Mozgova, I., Prochazkova Schrumpfova, P., Wimmerova, M., and Fajkus, J. (2009). Single-Myb-histone proteins from *Arabidopsis thaliana*: a quantitative study of telomere-binding specificity and kinetics. Biochem J. **419:** 221–228.

Kim, S.Y., Lee, J., Eshed-Williams, L., Zilberman, D., and Sung, Z.R. (2012). EMF1 and PRC2 cooperate to repress key regulators of Arabidopsis development. PLoS Genet. **8:** e1002512.

Kotake, T., Takada, S., Nakahigashi, K., Ohto, M., and Goto, K. (2003). Arabidopsis TERMINAL FLOWER 2 gene encodes a heterochromatin protein 1 homolog and represses both FLOWERING LOCUS T to regulate flowering time and several floral homeotic genes. Plant Cell Physiol. **44:** 555–564.

Kuchar, M., and Fajkus, J. (2004). Interactions of putative telomere-binding proteins in *Arabidopsis thaliana*: identification of functional TRF2 homolog in plants. FEBS Lett. **578:** 311–315.

Kumar, S.V., and Wigge, P.A. (2010). H2A.Z-containing nucleosomes mediate the thermosensory response in Arabidopsis. Cell **140:** 136–147.

Lafos, M., Kroll, P., Hohenstatt, M.L., Thorpe, F.L., Clarenz, O., and Schubert, D. (2011). Dynamic regulation of H3K27 trimethylation during Arabidopsis differentiation. PLoS Genet. **7:** e1002040.

Larsson, A.S., Landberg, K., and Meeks-Wagner, D.R. (1998). The TERMINAL FLOWER2 (TFL2) gene controls the reproductive transition and meristem identity in *Arabidopsis thaliana*. Genetics **149:** 597–605.

Li, C., Chen, C., Gao, L., Yang, S., Nguyen, V., Shi, X., Siminovitch, K., Kohalmi, S.E., Huang, S., Wu, K., Chen, X., and Cui, Y. (2015). The Arabidopsis SWI2/SNF2 chromatin Remodeler BRAHMA regulates polycomb function during vegetative development and directly activates the flowering repressor gene SVP. PLoS Genet. **11:** e1004944.

Libault, M., Tessadori, F., Germann, S., Snijder, B., Fransz, P., and Gaudin, V. (2005). The Arabidopsis LHP1 protein is a component of euchromatin. Planta **222:** 910–925.

Liu, C., Xi, W., Shen, L., Tan, C., and Yu, H. (2009). Regulation of floral patterning by flowering time genes. Dev. Cell **16:** 711–722.

Machanick, P., and Bailey, T.L. (2011). MEME-ChIP: motif analysis of large DNA datasets. Bioinformatics **27:** 1696–1697.

Margueron, R., and Reinberg, D. (2011). The Polycomb complex PRC2 and its mark in life. Nature **469:** 343–349.

Mirny, L.A. (2010). Nucleosome-mediated cooperativity between transcription factors. Proc. Natl. Acad. Sci. USA **107:** 22534–22539.

Moyle-Heyrman, G., Tims, H.S., and Widom, J. (2011). Structural constraints in collaborative competition of transcription factors against the nucleosome. J. Mol. Biol. **412:** 634–646.

Mozgova, I., and Hennig, L. (2015). The polycomb group protein regulatory network. Annu. Rev. Plant Biol. **66:** 269–296.

Mylne, J.S., Barrett, L., Tessadori, F., Mesnage, S., Johnson, L., Bernatavichute, Y.V., Jacobsen, S.E., Fransz, P., and Dean, C. (2006). LHP1, the Arabidopsis homologue of HETEROCHROMATIN PROTEIN1, is required for epigenetic silencing of FLC. Proc. Natl. Acad. Sci. USA **103:** 5012–5017.

Nakahigashi, K., Jasencakova, Z., Schubert, I., and Goto, K. (2005). The Arabidopsis heterochromatin protein1 homolog (TERMINAL FLOWER2) silences genes within the euchromatic region but not genes positioned in heterochromatin. Plant Cell Physiol. **46:** 1747–1756.

Platt, J.M., et al. (2013). Rap1 relocalization contributes to the chromatin-mediated gene expression profile and pace of cell senescence. Genes Dev. **27:** 1406–1420.

Quinlan, A.R., and Hall, I.M. (2010). BEDTools: a flexible suite of utilities for comparing genomic features. Bioinformatics **26:** 841–842.

Reimer, J.J., and Turck, F. (2010). Genome-wide mapping of protein-DNA interaction by chromatin immunoprecipitation and DNA microarray hybridization (ChIP-chip). Part A: ChIP-chip molecular methods. Methods Mol. Biol. **631:** 139–160.

Rice, P., Longden, I., and Bleasby, A. (2000). EMBOSS: the European Molecular Biology Open Software Suite. Trends Genet. **16:** 276–277.

Riha, K., McKnight, T.D., Griffing, L.R., and Shippen, D.E. (2001). Living with genome instability: plant responses to telomere dysfunction. Science **291:** 1797–1800.

Riha, K., and Shippen, D.E. (2003). Ku is required for telomeric C-rich strand maintenance but not for end-to-end chromosome fusions in Arabidopsis. Proc. Natl. Acad. Sci. USA **100:** 611–615.

Ruiz-Herrera, A., Nergadze, S.G., Santagostino, M., and Giulotto, E. (2008). Telomeric repeats far from the ends: mechanisms of origin and role in evolution. Cytogenet. Genome Res. **122:** 219–228.

Saldanha, A.J. (2004). Java Treeview–extensible visualization of microarray data. Bioinformatics **20:** 3246–3248.

Satake, A., and Iwasa, Y. (2012). A stochastic model of chromatin modification: cell population coding of winter memory in plants. J. Theor. Biol. **302:** 6–17.

Schrumpfova, P., Kuchar, M., Mikova, G., Skrisovska, L., Kubicarova, T., and Fajkus, J. (2004). Characterization of two *Arabidopsis thaliana* myb-like proteins showing affinity to telomeric DNA sequence. Genome **47:** 316–324.

Schrumpfova, P.P., Vychodilova, I., Dvorackova, M., Majerska, J., Dokladal, L., Schorova, S., and Fajkus, J. (2014). Telomere repeat binding proteins are functional components of Arabidopsis telomeres and interact with telomerase. Plant J. **77:** 770–781.

Schuettengruber, B., and Cavalli, G. (2009). Recruitment of polycomb group complexes and their role in the dynamic regulation of cell fate choice. Development **136:** 3531–3542.

Searle, I., He, Y., Turck, F., Vincent, C., Fornara, F., Kröber, S., Amasino, R.A., and Coupland, G. (2006). The transcription factor

FLC confers a flowering response to vernalization by repressing meristem competence and systemic signaling in Arabidopsis. Genes Dev. **20:** 898–912.

Sequeira-Mendes, J., Aragüez, I., Peiró, R., Mendez-Giraldez, R., Zhang, X., Jacobsen, S.E., Bastolla, U., and Gutierrez, C. (2014). The functional topography of the Arabidopsis genome is irganized in a reduced number of linear motifs of chromatin states. Plant Cell **26:** 2351–2366.

Shen, L., Shao, N., Liu, X., and Nestler, E. (2014). ngs.plot: Quick mining and visualization of next-generation sequencing data by integrating genomic databases. BMC Genomics **15:** 284.

Sung, S., He, Y., Eshoo, T.W., Tamada, Y., Johnson, L., Nakahigashi, K., Goto, K., Jacobsen, S.E., and Amasino, R.M. (2006). Epigenetic maintenance of the vernalized state in *Arabidopsis thaliana* requires LIKE HETEROCHROMATIN PROTEIN 1. Nat. Genet. **38:** 706–710.

Takada, S., and Goto, K. (2003). Terminal flower2, an Arabidopsis homolog of heterochromatin protein1, counteracts the activation of flowering locus T by constans in the vascular tissues of leaves to regulate flowering time. Plant Cell **15:** 2856–2865.

Tremousaygue, D., Garnier, L., Bardet, C., Dabos, P., Herve, C., and Lescure, B. (2003). Internal telomeric repeats and 'TCP domain' protein-binding sites co-operate to regulate gene expression in *Arabidopsis thaliana* cycling cells. Plant J. **33:** 957–966.

Turck, F., Roudier, F., Farrona, S., Martin-Magniette, M.L., Guillaume, E., Buisine, N., Gagnot, S., Martienssen, R.A., Coupland, G., and Colot, V. (2007). Arabidopsis TFL2/LHP1 specifically associates with genes marked by trimethylation of histone H3 lysine 27. PLoS Genet. **3:** e86.

Vaquero-Sedas, M.I., and Vega-Palas, M.A. (2011). On the chromatin structure of eukaryotic telomeres. Epigenetics **6:** 1055–1058.

Wang, H., Liu, C., Cheng, J.X., Liu, J., Zhang, L., He, C., Shen, W.H., Jin, H., Xu, L., and Zhang, Y. (2016). Arabidopsis flower and embryo developmental genes are repressed in seedlings by different combinations of Polycomb Group proteins in association with distinct sets of cis-regulatory elements. PLoS Genet. **12:** e1005771.

Weinhofer, I., Hehenberger, E., Roszak, P., Hennig, L., and Köhler, C. (2010). H3K27me3 profiling of the endosperm implies exclusion of polycomb group protein targeting by DNA methylation. PLoS Genet. **6:** 6.

Welchen, E., and Gonzalez, D.H. (2005). Differential expression of the Arabidopsis cytochrome c genes Cytc-1 and Cytc-2. Evidence for the involvement of TCP-domain protein-binding elements in anther- and meristem-specific expression of the Cytc-1 gene. Plant Physiol. **139:** 88–100.

Xiao, J., and Wagner, D. (2015). Polycomb repression in the regulation of growth and development in Arabidopsis. Curr. Opin. Plant Biol. **23:** 15–24.

Xu, L., and Shen, W.H. (2008). Polycomb silencing of KNOX genes confines shoot stem cell niches in Arabidopsis. Curr. Biol. **18:** 1966–1971.

Yang, C., Bratzel, F., Hohmann, N., Koch, M., Turck, F., and Calonje, M. (2013). VAL- and AtBMI1-mediated H2Aub initiate the switch from embryonic to postgerminative growth in Arabidopsis. Curr. Biol. **23:** 1324–1329.

Yang, D., Xiong, Y., Kim, H., He, Q., Li, Y., Chen, R., and Songyang, Z. (2011). Human telomeric proteins occupy selective interstitial sites. Cell Res. **21:** 1013–1027.

Ye, J., Renault, V.M., Jamet, K., and Gilson, E. (2014). Transcriptional outcome of telomere signalling. Nat. Rev. Genet. **15:** 491–503.

Zang, C., Schones, D.E., Zeng, C., Cui, K., Zhao, K., and Peng, W. (2009). A clustering approach for identification of enriched domains from histone modification ChIP-Seq data. Bioinformatics **25:** 1952–1958.

Zhang, H., Bishop, B., Ringenberg, W., Muir, W.M., and Ogas, J. (2012). The CHD3 remodeler PICKLE associates with genes enriched for trimethylation of histone H3 lysine 27. Plant Physiol. **159:** 418–432.

Zhang, X., Clarenz, O., Cokus, S., Bernatavichute, Y.V., Pellegrini, M., Goodrich, J., and Jacobsen, S.E. (2007b). Whole-genome analysis of histone H3 lysine 27 trimethylation in Arabidopsis. PLoS Biol. **5:** e129.

Zhang, X., Germann, S., Blus, B.J., Khorasanizadeh, S., Gaudin, V., and Jacobsen, S.E. (2007a). The Arabidopsis LHP1 protein colocalizes with histone H3 Lys27 trimethylation. Nat. Struct. Mol. Biol. **14:** 869–871.